Structural stability and lattice defects in copper: *Ab initio*, tight-binding, and embedded-atom calculations

Y. Mishin
School of Computational Sciences, George Mason University, Fairfax, Virginia 22030

M. J. Mehl and D. A. Papaconstantopoulos
Center for Computational Materials Science, Naval Research Laboratory, Washington, DC 20375-5345

A. F. Voter and J. D. Kress
Theoretical Division, Los Alamos National Laboratory, Los Alamos, New Mexico 87545

(Received 13 December 2000; published 21 May 2001)

We evaluate the ability of the embedded-atom method (EAM) potentials and the tight-binding (TB) method to predict reliably energies and stability of nonequilibrium structures by taking Cu as a model material. Two EAM potentials are used here. One is constructed in this work by using more fitting parameters than usual and including *ab initio* energies in the fitting database. The other potential was constructed previously using a traditional scheme. Excellent agreement is observed between *ab initio*, TB, and EAM results for the energies and stability of several nonequilibrium structures of Cu, as well as for energies along deformation paths between different structures. We conclude that not only TB calculations but also EAM potentials can be suitable for simulations in which correct energies and stability of different atomic configurations are essential, at least for Cu. The bcc, simple cubic, and diamond structures of Cu were identified as elastically unstable, while some other structures (e.g., hcp and 9R) are metastable. As an application of this analysis, nonequilibrium structures of epitaxial Cu films on (001)-oriented fcc or bcc substrates are evaluated using a simple model and atomistic simulations with an EAM potential. In agreement with experimental data, the structure of the film can be either deformed fcc or deformed hcp. The bcc structure cannot be stabilized by epitaxial constraints.

DOI: 10.1103/PhysRevB.63.224106 PACS number(s): 61.50.Ah, 61.50.Ks, 61.72.Bb, 64.70.Kb

I. INTRODUCTION

The energetics and mechanical stability of nonequilibrium structures of metals are important in many problems, such as phase diagram construction, structure of grain boundaries, or epitaxial thin films. The most interesting finding is that many of such ''excited'' phases, although close to the ground-state structure in energy, turn out to be unstable against homogeneous shear deformation or certain phonon modes.[1,2] For example, it was found by *ab initio* calculations that the bcc and simple cubic (sc) structures of many fcc metals are unstable against tetragonal and trigonal deformations, respectively.[1–9] Likewise, the fcc structure of bcc metals was found to be unstable against tetragonal distortions.[1,2] These instabilities have implications for the phase diagram construction by empirical methods, in which such phases are treated as metastable (i.e., stable against any small distortion).[1,2,10]

Some of the ''excited'' structures were found in core regions of extended defects and in epitaxial thin films. For example, a thin ($\sim$1 nm) layer of the 9R phase was predicted by atomistic simulations and observed by high-resolution electron microscopy at $\Sigma=3$ [110] tilt grain boundaries in fcc Ag and Cu.[11,12] Other $\Sigma=3$ boundaries in Cu were predicted, and experimentally found, to form a thin layer of the bcc structure.[13,14] The experimentally observed structure of Cu layers grown epitaxially on (001) substrates is often interpreted as bcc,[15,16] although other authors consider it as strongly deformed fcc.[6,7] Hcp Cu was also found in epitaxial films grown on W(100). The latter observation is easier to comprehend since hcp is a truly metastable phase of bulk Cu. In this and similar cases, a transformation of the metastable phase to the ground state can be prevented by constraints imposed on the metastable layer by the substrate. The unstable bcc structure presents a conceptually different case. Although it cannot be excluded that a bcc structure consisting of just a few monolayers does not possess the instability inherent to a bulk bcc crystal, a thicker bcc layer can hardly be stabilized by any constraints and should transform to the ground-state fcc structure or some truly metastable phase. It has not been determined until now whether the 9R structure of fcc metals is metastable. If so, it can be stabilized in epitaxial films and at grain boundaries by the same mechanism as the hcp phase.

While the energies and stability of various crystalline structures of metals can be calculated by *ab initio* methods, computational limitations prevent such methods from being applied to atomistic simulations of constrained structures appearing in thin films and around extended defects. Faster methods based on fitting parameters, such as the tight-binding (TB) approximation[17,18] and especially the embedded-atom method (EAM),[19] are more suitable for this purpose. However, it is currently not totally understood how reliable such schemes are in representing the energies and stability of structures away from the ground state. It has been demonstrated for a number of fcc, bcc, and hcp metals that the TB method can successfully reproduce the energy differences between the ground-state and nonequilibrium structures not included in the fit.[18] The elastic instability of nonequilibrium fcc, bcc, and sc structures is also reproduced by

the TB method correctly.[18] Furthermore, it has been shown that EAM potentials for Ni and Al constructed by including *ab initio* data in the fitting database are successful in predicting the structural energy differences between various phases and the instability of the bcc and sc structures.[8,20] Such potentials also demonstrate good agreement with *ab initio* energies along tetragonal and trigonal deformation paths between fcc, bcc, and sc structures. However, the transferability of TB and EAM methods to other deformation paths has not been evaluated so far, and the stability of structures other than fcc, bcc, and sc has not been studied by either *ab initio*, TB, or EAM methods.

In this paper we continue our investigations in this direction, using Cu as a prototype. We first (Sec. II) generate a database of *ab initio* energies of various crystalline structures of Cu as functions of volume, together with energies along several deformation paths between the structures. Part of the structural energies are used for fitting the TB parameters for Cu. In Sec. III we introduce two EAM potentials for Cu. One potential is constructed by the scheme introduced in Refs. 8 and 20 based on both experimental data and *ab initio* structural energies. We also use this potential generation as an opportunity to address the long-standing problem with EAM potentials. Namely, such potentials are normally optimized for properties that are determined by atomic interactions at distances close to equilibrium or larger. Interactions at shorter distances are obtained by an arbitrary extrapolation, and are often less than reliable. In this work, the short-range parts of the potential functions are fit to reproduce *ab initio* energies of the fcc phase and a diatomic molecule (dimer) of Cu at very short atomic separations, including repulsion energies in the keV range. The potential is expected to have an improved reliability in atomistic simulations involving short atomic separations, such as surface sputtering, shock waves, etc. The second potential was constructed previously[21,22] using a traditional scheme based on experimental data only. Other EAM potentials for Cu can be found in the literature (see, e.g., Refs. 23–29). It is not our purpose to analyze their qualities. Rather, we choose to construct a potential based on our fitting scheme,[8,20] take a traditional potential[21,22] for comparison, and evaluate the capability of the EAM, represented by these two potentials, to predict structural energies and stability of ''excited'' phases of Cu in comparison with such capabilities of the TB and *ab initio* methods. The phases considered here include, besides the previously analyzed fcc, bcc, and sc structures, five more ''excited'' phases. In Sec. VI we compare the energies along several deformation paths calculated by *ab initio*, TB, and EAM methods. Such calculations provide not only a test of the EAM potentials but also information about mechanical (in)stability of different phases. As an application of our analysis, the structure of epitaxial Cu films on a fcc(100) substrate is evaluated in Sec. VII using an EAM potential. In Sec. VIII we summarize.

II. *Ab initio* AND TIGHT-BINDING CALCULATIONS

Most of the *ab initio* structural energies were generated using the first-principles general-potential linearized augmented plane wave (LAPW) method.[30,31] The electronic exchange and correlation was specified by the Perdew-Wang parametrization[32] of the local density approximation (LDA) within the Kohn-Sham formulation of the density functional theory.[33] The core states of the Cu atom were treated fully relativistically in a spherically symmetric potential. The $3d$ and $4s$ valence electrons were treated in the semirelativistic approximation,[34] i.e., without spin-orbit interactions. Brillouin zone integrations were performed using a regularly spaced set of **k**-points which included the origin. To speed convergence, we follow Gillan[35] and smear out the electronic eigenvalues with a Fermi distribution at $T=5$ mRy. We carefully checked the convergence of the **k** point mesh.[36,37] We also used a rather large basis set, with approximately 150 basis functions per atom at the equilibrium volume. We estimate that the energies are converged to better than 0.5 mRy/atom.

The fcc energies were also calculated in the generalized gradient approximation (GGA) of the density-functional theory with the VASP program, which was developed at the Technical University of Vienna.[38–40] The Perdew-Wang 91 parametrization of the GGA (Ref. 41) and a plane-wave basis set with a cutoff of $E_{cut}=26$ Ry were employed. The core states of Cu were represented with a Vanderbilt ultrasoft pseudopotential[42] in a form supplied by G. Kresse and J. Hafner.[43] Convergence with respect to both the **k**-point mesh and the value of E_{cut} were carefully checked. For the fcc structure, the equilibrium lattice period $a_0=3.642$ Å, and the bulk modulus $B=1.38\times10^{11}$ Pa were obtained. Also, the cohesive energy of the bcc structure was 0.04 eV higher than that for fcc. Cu dimer energies were calculated with the hybrid density-functional theory (the Becke exchange[44] and the Lee-Yang-Parr correlation[45,46] functionals, so-called B3LYP) using the Gaussian98 suite of programs.[47] An all-electron Gaussian basis set (6-311G) provided converged results. Both fcc and dimer calculations extended to short interatomic distances corresponding to energies in the keV range.

The Naval Research Laboratory (NRL) TB method used in this work is discussed in detail in Ref. 18. In this method the TB Hamiltonian is determined by a least-squares fit to the total energy and the energy bands of LAPW calculations described above. In the present case the LAPW database included the fcc, bcc, and sc structures for a wide range of volumes. The energy bands were fitted with a root-mean-square error of 5 mRy and the total energy with an accuracy of 0.5 mRy. During the fit a block diagonilization of the TB Hamiltonian at high symmetry points was used to avoid the possibility of incorrectly assigning the symmetry and angular momentum character to different states. Care was taken to include energies at very small atomic volumes (down to 60% of the equilibrium value). It should be stressed that no experimental data was used to determine the TB parameters. As will be discussed in subsequent sections of the article, these parameters are well transferable to other structures not included in the fit.[48]

The NRL-TB method is computationally very efficient. For systems including *s*, *p*, and *d* orbitals, TB calculations are approximately 1000 times faster than LAPW calculations. This allows for generating, for example, phonon dispersion curves (discussed below in this paper) very quickly.

Recently, the NRL-TB method has been used to perform molecular dynamics (MD) simulations for 343 atoms with 3000 MD steps, an almost impossible task with the LAPW method.[49,50] In particular, such MD simulations were applied to calculate the thermal expansion of fcc Au and the pair correlation function of liquid Au. They were also applied to calculate the vibrational density of states (DOS) of crystalline Si and the electronic DOS of amorphous Si using a 1728-atom supercell. Since the emphasis of this paper is on the EAM, these and other applications of the NRL-TB method are not discussed here in detail, but the interested reader can find further details in Refs. 49 and 50.

To facilitate a comparison with EAM calculations, all *ab initio* structural energies were shifted[8] by the same amount so as to make the equilibrium fcc energy coincide with the experimental cohesive energy of -3.54 eV/atom. Due to this shift we can talk about structural energies rather than structural energy differences.[51] Likewise, all interatomic distances involved in the LDA calculations were scaled[8] to make the equilibrium lattice spacing of the fcc phase coincide with the experimental value of 3.615 Å . This scaling takes into account that LDA calculations tend to underestimate interatomic distances in the equation of state of a crystal. Because the TB parameters are fit to the LDA energies and distances, all TB data were subject to the same kind of shifting and scaling as the LDA data. The energies of a Cu dimer were compared with EAM energies directly.

III. PARAMETRIZATION AND FITTING OF EAM POTENTIALS

In the embedded-atom method,[19,52] the total energy of an elemental system is represented as

$$E_{\rm tot}=\frac{1}{2}\sum_{ij} V(r_{ij})+\sum_i F(\bar{\rho}_i). \tag{1}$$

Here $V(r_{ij})$ is a pair potential as a function of distance r_{ij} between atoms i and j, and F is the embedding energy as a function of the host electron density $\bar{\rho}_i$ induced at site i by all other atoms in the system. The latter is given by

$$\bar{\rho}_i=\sum_{j\neq i} \rho(r_{ij}), \tag{2}$$

where $\rho(r)$ is the electron density function. While the functional form of Eq. (1) is based on certain physical ideas regarding bonding in metallic systems, the potential functions $V(r)$, $\rho(r)$, and $F(\bar{\rho})$ have practically lost their ties with the original physical meaning and are treated as some fitting functions that can be parametrized any reasonable way with the only requirement that the potential should work. Two EAM potentials, constructed in different ways and called here EAM1 and EAM2, will be compared in this paper.

The potential EAM1 was generated using the scheme introduced in Ref. 20 and slightly modified here. In this scheme, the potential is generated directly in the effective pair format.[53] The pair interaction function is parametrized as

$$V(r)=[E_1M(r,r_0^{(1)},\alpha_1)+E_2M(r,r_0^{(2)},\alpha_2)+\delta]\times\psi\left(\frac{r-r_{\rm c}}{h}\right)-\sum_{n=1}^{3} H(r_{\rm s}^{(n)}-r)S_n(r_{\rm s}^{(n)}-r)^4, \tag{3}$$

where

$$M(r,r_0,\alpha)=\exp[-2\alpha(r-r_0)]-2\exp[-\alpha(r-r_0)] \tag{4}$$

is a Morse function and $H(x)$ is a unit step function. Equation (3) includes a cutoff function $\psi(x)$ defined as $\psi(x)=0$ if $x\geqslant 0$ and $\psi(x)=x^4/(1+x^4)$ if $x<0$. The last term in Eq. (3) is added to control the strength of pairwise repulsion between atoms at short distances. Eq. (3) contains 15 fitting parameters: E_1, E_2, $r_0^{(1)}$, $r_0^{(2)}$, α_1, α_2, δ, $r_{\rm c}$, h, and $\{r_{\rm s}^{(n)},S_n\}_{n=1,2,3}$.

The electron density function is taken in the form

$$\rho(r)=[a\exp(-\beta_1(r-r_0^{(3)})^2)+\exp(-\beta_2(r-r_0^{(4)}))]\times\psi\left(\frac{r-r_{\rm c}}{h}\right), \tag{5}$$

with 5 more fitting parameters: a, $r_0^{(3)}$, $r_0^{(4)}$, β_1, and β_2. The cutoff function $\psi(x)$ guarantees that functions $V(r)$, $\rho(r)$ and their derivatives up to the second one turn to smoothly zero at the cutoff distance $r_{\rm c}$.

The function $\rho(r)$ is normalized to $\bar{\rho}=1$ in the equilibrium fcc crystal,

$$\bar{\rho}=\sum_m N_m\rho_m=1. \tag{6}$$

The function $V(r)$ is also required to satisfy the mechanical equilibrium condition of the fcc crystal at the experimental lattice period a_0,

$$\sum_m N_mR_mV_m'=0. \tag{7}$$

Equations (6) and (7) use the notations $V_m=V(R_m)$ and $\rho_m=\rho(R_m)$, where R_m and N_m are the radius and the number of atoms at the mth coordination shell. These equations can be easily solved for a and E_1, respectively, which reduces the number of free fitting parameters by 2.

The embedding function is represented by a polynomial

$$F(\bar{\rho})=F^{(0)}+\frac{1}{2}F^{(2)}(\bar{\rho}-1)^2+\sum_{n=1}^{4} q_n(\bar{\rho}-1)^{n+2} \tag{8}$$

for $\bar{\rho}<1$ and

$$F(\bar{\rho})=\frac{F^{(0)}+\frac{1}{2}F^{(2)}(\bar{\rho}-1)^2+q_1(\bar{\rho}-1)^3+Q_1(\bar{\rho}-1)^4}{1+Q_2(\bar{\rho}-1)^3} \tag{9}$$

for $\bar{\rho}>1$. The denominator in Eq. (9) guarantees that $F(\bar{\rho})$ increases no faster than linearly in the regime of very large densities at which atomic interactions are dominated by

strong pairwise repulsion. The coefficients $F^{(0)}$ and $F^{(2)}$ can be expressed in terms of the experimental values of the cohesive energy E_0 and bulk modulus B,[8,20]

$$F^{(0)}=E_0-\frac{1}{2}\sum_m N_m V_m, \tag{10}$$

$$\frac{1}{2}\sum_m N_m V_m'' R_m^2+F^{(2)}\left(\sum_m N_m \rho_m' R_m\right)^2=9B\Omega_0, \tag{11}$$

Ω_0 being the equilibrium atomic volume. Furthermore, the coefficient q_1, can be determined from the boundary condition $F(0)=0$. Then, only the coefficients q_2, q_3, q_4, Q_1 and Q_2 can be used as free fitting parameters for $F(\bar{\rho})$. Overall, this parametrization of the potential includes 23 free parameters. Note that this fitting scheme automatically guarantees an exact fit to a_0, E_0, and B.

The potential was optimized by minimizing the weighted mean squared deviation of selected properties of Cu from their target values taken from experiments or obtained by *ab initio* calculations. The weights served to control the relative importance of different properties.[8,20] Besides a_0, E_0, and B, the experimental part of the fitting database contained the elastic constants c_{ij}, the phonon frequencies $\nu_L(X)$ and $\nu_T(X)$ at the zone-boundary point X, the relaxed vacancy formation (E_f) and migration (E_m) energies, and the intrinsic stacking fault energy γ_{SF}. Thermal expansion factors of fcc Cu at several temperatures and the equilibrium bond energy (E_d) of a Cu dimer were also included with a small weight. Additionally, the fcc structural energy was required to follow the universal equation of state of Rose *et al.* [54] around the equilibrium as accurately as possible. The *ab initio* part of the database contained the excess energies of the hcp and bcc structures over fcc. All other *ab initio* data were deferred for testing the potential. The short-r part of the potential was optimized separately, through parameters $\{r_s^{(n)},S_n\}_{n=1,2,3}$ and Q, to reproduce the *ab initio* energies of the fcc structure and a dimer under strong compressions.

The potential EAM2 was constructed previously using a more traditional scheme.[21,22] The pair interaction was described by a Morse function,

$$V(r)=E_1 M(r,r_0,\alpha) \tag{12}$$

[see Eq. (4)], while the electron density function was taken as the density of a hydrogenic $4s$ orbital,

$$\rho(r)=r^6(e^{-\beta r}+2^9 e^{-2\beta r}). \tag{13}$$

Following Foiles,[55] the embedding function $F(\bar{\rho})$ was defined by requiring that the fcc energy exactly follow the universal equation of state of Rose *et al.*[54] This scheme also gives a perfect agreement with experimental values of a_0, E_0, and B. To provide a smooth cutoff, the above expressions for $V(r)$ and $\rho(r)$ are modified to make them go to zero together with their first derivatives at $r\to r_c$ (see Refs. 21 and 52 for details). This scheme contains only five fitting parameters, which are optimized to the experimental values of c_{ij}, the unrelaxed vacancy formation energy, and the equilibrium bond energy (E_d) and length (R_d) of a Cu dimer, subject to the requirement that the fcc structure be more stable than hcp and bcc.

TABLE I. Optimized parameters of the potential EAM1.

Parameter	Value	Parameter	Value
r_c (Å)	5.50679	S_3 (eV/Å^4)	1.15000×10^3
h (Å)	0.50037	a	3.80362
E_1 (eV)	2.01458×10^2	$r_0^{(3)}$ (Å)	−2.19885
E_2 (eV)	6.59288×10^{-3}	$r_0^{(4)}$ (Å)	-2.61984×10^2
$r_0^{(1)}$ (Å)	0.83591	β_1 (Å^{-2})	0.17394
$r_0^{(2)}$ (Å)	4.46867	β_2 (Å^{-1})	5.35661×10^2
α_1 (Å^{-1})	2.97758	$F^{(0)}$ (eV)	−2.28235
α_2 (Å^{-1})	1.54927	$F^{(2)}$ (eV)	1.35535
δ (Å)	0.86225×10^{-2}	q_1 (eV)	−1.27775
$r_s^{(1)}$ (Å)	2.24000	q_2 (eV)	−0.86074
$r_s^{(2)}$ (Å)	1.80000	q_3 (eV)	1.78804
$r_s^{(3)}$ (Å)	1.20000	q_4 (eV)	2.97571
S_1 (eV/Å^4)	4.00000	Q_1	0.40000
S_2 (eV/Å^4)	40.00000	Q_2	0.30000

Tables I and II summarize the optimized parameters of the potentials, while Fig. 1 shows the potential functions. Note that the EAM2 potential has been transformed to the effective pair format for comparison. Despite the different parametrization and fitting schemes, both sets of potential functions look similar except in the short-r (large $\bar{\rho}$) range. While the EAM2 potential limits atomic interactions to three coordination shells, the EAM1 potential includes also the fourth coordination shell. The effective pair interaction with the fourth coordination shell is repulsive and very small ($\sim10^{-3}$ eV). The potential functions in the tabulated form are available via the World Wide Web[56] or by Email from the authors.

IV. TESTING THE EAM POTENTIALS

A. Lattice properties

Table III demonstrates that both potentials provide an accurate match to the experimental elastic constants and phonon frequencies in the equilibrium fcc lattice of Cu. (We note that the EAM2 potential was fit to slightly different experimental values of c_{ij}.[21]) The potentials show good agreement with experimental phonon dispersion curves,[57] especially the EAM1 potential (Fig. 2). Although only the frequencies at the zone-boundary point X were included in the fit, all other frequencies are reproduced rather accurately. Some deviations are observed in the high-frequency range (>7 THz). An agreement with experimental phonon fre-

TABLE II. Optimized parameters of the potential EAM2 (Ref. 21).

E_1 (eV)	r_0 (Å)	α (Å^{-1})	β (Å^{-1})	r_c (Å)
0.7366	2.3250	1.9190	4.0430	4.9610

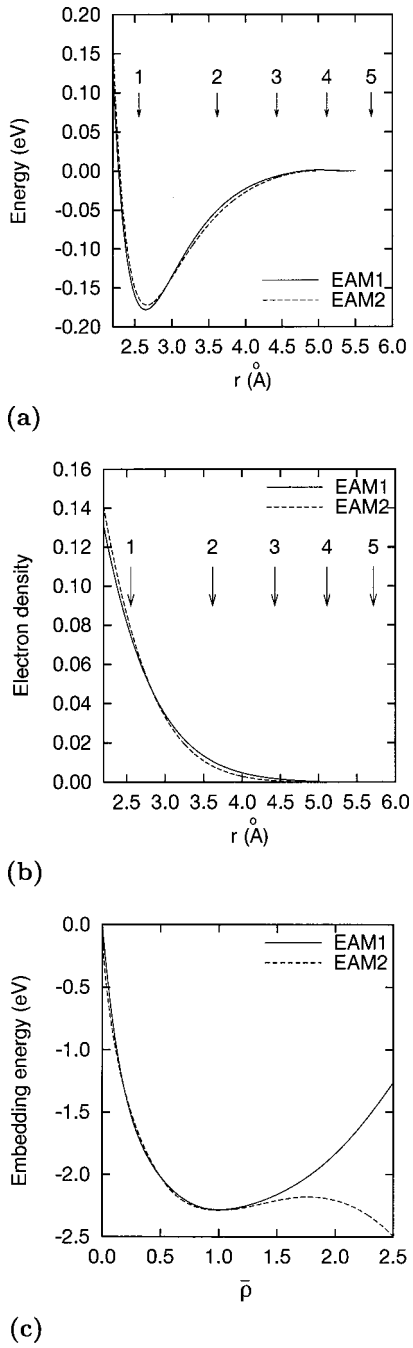

FIG. 1. Potential functions for the EAM1 and EAM2 potentials: (a) pair interaction function, (b) electron density function, and (c) embedding function. The arrows indicate coordination radii in fcc lattice.

quencies is an important quality of potentials, and was even suggested as a criterion of their global reliability.[58] Phonon frequencies were also calculated by the TB method using an $11\times11\times11$ supercell. Although no phonon data were included in the TB fit, the agreement with experimental data is rather good (Fig. 2).

Thermal expansion factors of fcc Cu were calculated by two methods: by minimizing the free energy of the crystal as a function of volume in the quasiharmonic approximation,[59] and by Metropolis Monte Carlo simulations[59,60] performed under zero pressure. Both calculations used a cubic supercell with 500 atoms. The EAM2 potential tends to overestimate the thermal expansion, while the EAM1 potential demonstrates significantly better agreement with experimental data (Fig. 3).

TABLE III. Lattice properties of Cu predicted by the EAM potentials in comparison with experimental data. * data not included in the fit.

	Experiment	EAM1	EAM2
a_0 (Å)	3.615[a]	3.615	3.615
E_0 (eV/atom)	−3.54[b]	−3.54	−3.54
B (10^{11} Pa)	1.383[c]	1.383	1.419
c_{11} (10^{11} Pa)	1.700[c]	1.699	1.793
c_{12} (10^{11} Pa)	1.225[c]	1.226	1.232
c_{44} (10^{11} Pa)	0.758[c]	0.762	0.810
$\nu_L(X)$ (THz)	7.38[d]	7.82	7.94*
$\nu_T(X)$ (THz)	5.16[d]	5.20	5.22*
$\nu_L(L)$ (THz)	7.44[d]	7.78*	7.93*
$\nu_T(L)$ (THz)	3.41[d]	3.32*	3.36*
$\nu_L(K)$ (THz)	5.90[d]	6.22*	6.37*
$\nu_{T_1}(K)$ (THz)	4.60[d]	4.65*	4.71*
$\nu_{T_2}(K)$ (THz)	6.70[d]	7.17*	7.30*

[a]Reference 77.
[b]Reference 79.
[c]Reference 80.
[d]Reference 57. The results in tabulated form can be found in Ref. 81.

B. Equation of state

Figure 4 presents the equation of state of fcc Cu (energy as a function of the first-neighbor distance under hydrostatic strain) calculated with the EAM potentials, in comparison

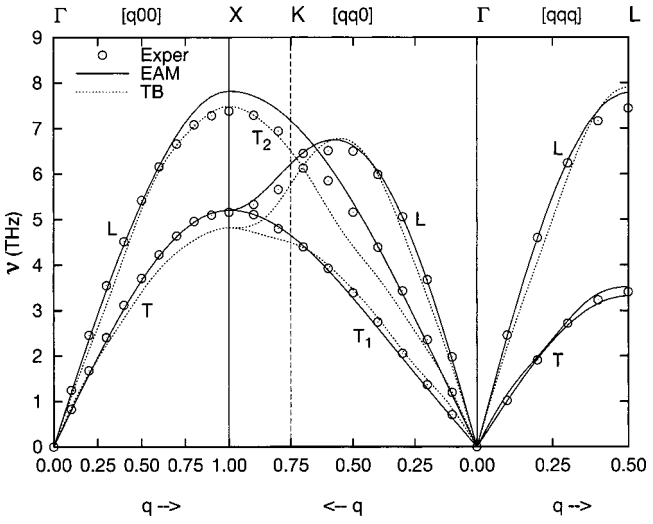

FIG. 2. Phonon dispersion curves calculated with the EAM1 potential and by the TB method. Experimental points (○) measured by neutron diffraction at temperature 80 K are shown for comparison (Ref. 57).

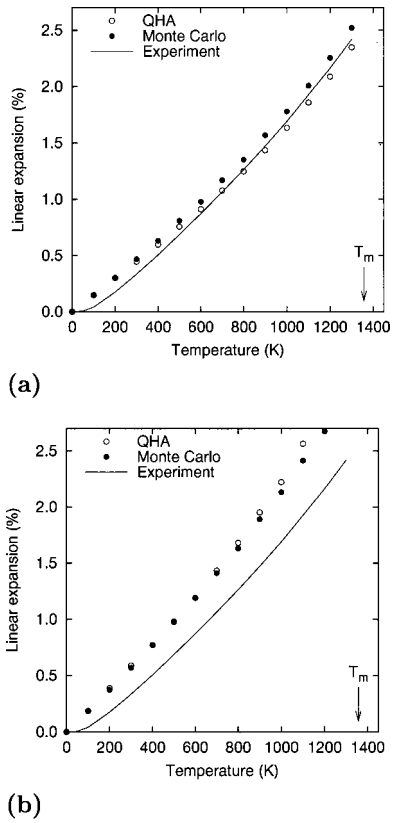

FIG. 3. Linear thermal expansion of Cu calculated in the quasiharmonic approximation (QHA) and by the Monte Carlo method using the EAM1 (a) and EAM2 (b) potentials. Experimental data (Ref. 92) are shown for comparison. The melting point of Cu (T_m) is indicated.

with *ab initio* and TB calculations. While good agreement is observed between all calculation methods around the equilibrium [Fig. 4(a)], discrepancies appear in the strongly compressive mode [Fig. 4(b)]. In this mode, the energies predicted by the EAM2 potential, which exactly follow Rose's universal equation of state[54] by construction, are significantly lower than *ab initio* energies. On the other hand, the TB energies tend to overestimate *ab initio* data in this regime. The EAM1 potential shows very good agreement with *ab initio* energies because such energies were included in the fitting database. Figure 4(b) demonstrates that Rose's equation of state may not be a good guide far away from equilibrium, and that it is more advantageous to use *ab initio* energies for optimizing interatomic potentials in the strongly compressive mode. As an additional confirmation, Fig. 5 demonstrates that the EAM1 potential provides a better agreement with the experimental pressures[61,62] under strong compressions than the EAM2 potential.

C. Lattice defects

Vacancies and interstitials in Cu were studied in a cubic supercell with $N=864$ atoms. The energy of defect formation, E_f, was determined as

$$E_f = E_{def} - (N \pm 1)E_0, \tag{14}$$

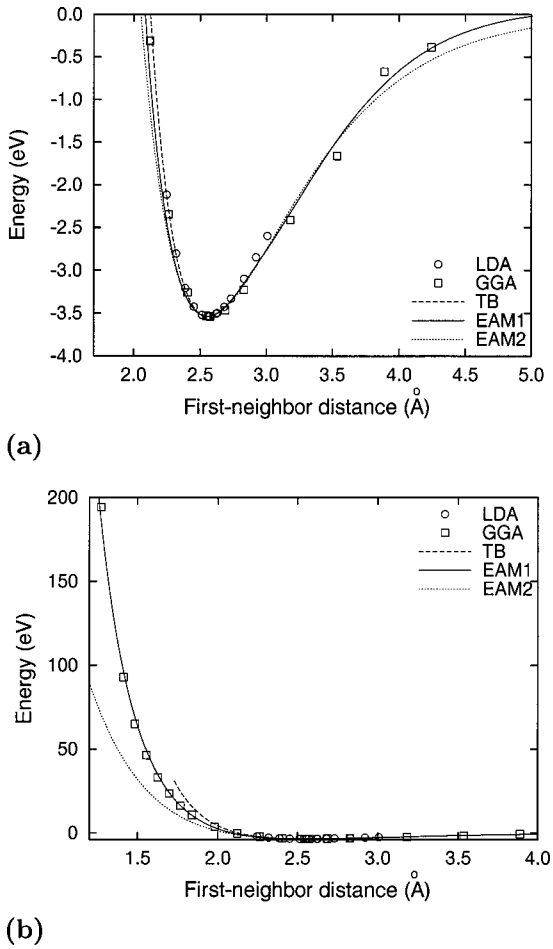

FIG. 4. Comparison of *ab initio* (○, □), TB, and EAM-calculated equations of state of fcc Cu. (a) Around equilibrium. (b) At short distances.

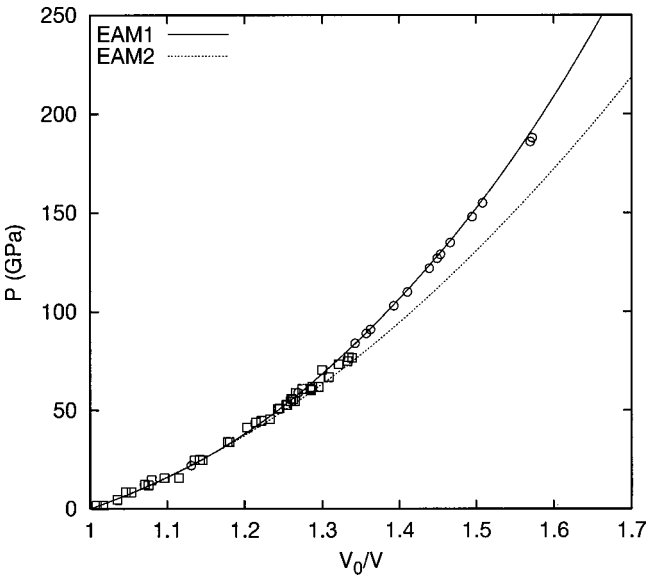

FIG. 5. Pressure-volume relation in Cu at $T=0$ calculated with the EAM potentials in comparison with experimental data (○, Ref. 61; □, Ref. 62).

where E_{def} is the energy of the relaxed supercell containing a single defect. The negative sign corresponds to a vacancy while a positive sign to an interstitial. During the relaxation, the volume of the supercell was allowed to vary in order to ensure zero pressure conditions. From the volume change due to the relaxation, V_r, the defect formation volume was determined as

$$\Omega_f = V_r \pm \Omega_0, \tag{15}$$

with a positive sign for a vacancy and a negative sign for an interstitial. For an interstitial, the split [001] dumbbell configuration was found to have the lowest energy. Moreover, [110] and [111] dumbbells were found to be unstable against rotations around the dumbbell center of mass.

The entropy of defect formation, S_f, was calculated in the harmonic approximation[59] from the change in the vibrational entropy of the supercell upon creation of a single defect. Similarly to Eq. (14),

$$S_f = S_{def} - (N \pm 1) S_{perf}/N, \tag{16}$$

where S_{def} and S_{perf} are the vibrational entropies of the defected and perfect supercells. When constructing the dynamical matrix, one of the atoms in the block was treated as static in order to eliminate the translational invariance of the potential energy.

Point defect migration was studied by molecular dynamics. As expected, a vacancy was found to move by exchanging positions with a nearest-neighbor atom. An interstitial was established to move between nearest-neighbor sites by translating the dumbbell center of mass with a simultaneous 90° rotation in the (100) plane containing the initial dumbbell and the destination site. The defect migration energy, E_m, and volume, Ω_m, were determined from the difference in the supercell energy (volume) at the saddle point and in the initial state. The saddle points were located by the nudged elastic band method.[63] The attempt frequency of point-defect migration, ν_0, was calculated within the harmonic transition state theory.[64]

Table IV compares EAM-predicted point defect characteristics with experimental data. For a vacancy, both potentials give reasonable agreement with experiments. The largest discrepancy is observed for the vacancy formation entropy, but it should be kept in mind that the experimental value of S_{def} is rather approximate.[65] Experimental data for interstitials are missing or unreliable owing to the extremely low equilibrium concentration and high mobility of interstitials. However, the observed agreement for the interstitial migration energy is encouraging.

The calculated intrinsic stacking fault and (111) twin energies are consistent with experimental data (Table V), with slightly better agreement for the EAM1 potential. Since the stacking fault energy determines the width of dislocation dissociation in the fcc lattice, the correct value of γ_{SF} is important for atomistic simulations of dislocations and fracture. Note that TB calculations underestimate γ_{SF}, but this quantity was not included in the TB fit. The unstable stacking fault energy, γ_{us}, is another important quantity involved in such simulations. This quantity enters the criterion of ductile versus brittle behavior of materials proposed by Rice.[66] It can be viewed as the activation barrier that should be overcome when an intrinsic stacking fault is created by shifting one half of the crystal relative to the other in $[\bar{2}11]$ direction along a (111) plane. The energy response to such shifts is best represented by the γ surface technique introduced by Vitek.[67,68] Figure 6 presents the relevant section of the γ

TABLE IV. Properties of point defects in Cu predicted by the EAM potentials in comparison with experimental data. k_B is the Boltzmann constant; other notations are explained in Sec. IV C.

	Experiment	EAM1	EAM2
Vacancy:			
E_f (eV)	1.27[a], 1.28[b]	1.272	1.258
Ω_f/Ω_0	0.78[c]	0.701	0.743
S_f/k_B	2.35[b]	1.404	1.245
E_m (eV)	0.71[b]	0.689	0.690
Ω_m/Ω_0	0.12[d]	0.107	0.166
ν_0 (THz)		7.69	16.22
Interstitial:			
E_f (eV)	2.8-4.2[e]	3.063	3.229
Ω_f/Ω_0	0.55 ± 0.20[e]	0.834	1.061
S_f/k_B		7.429	11.00
E_m (eV)	0.12[f]	0.098	0.083
Ω_m/Ω_0		0.041	0.038
ν_0 (THz)		1.20	1.36

[a]Reference 82.
[b]Reference 65.
[c]Reference 83.
[d]Evaluated from the experimental result $\Omega_f + \Omega_m \approx 0.9\Omega_0$ [pressure dependence of self-diffusion (Refs. 84 and 85)] and using $\Omega_f = 0.78\Omega_0$ (Ref. 83).
[e]Reference 86.
[f]Reference 87.

TABLE V. Energies (γ, in mJ/m^2) of planar defects in Cu predicted by the EAM potentials in comparison with experimental data and TB calculations. SF: intrinsic stacking fault; us: unstable stacking fault; GB: $\Sigma=5$ symmetrical tilt grain boundary with tilt axis [001] and boundary plane (210) or (310); s: surface with orientations (111), (110), or (100); *T*: symmetrical twin. TB calculations were performed in a 24 atom supercell.

	Experiment	TB	EAM1	EAM2
γ_{SF}	45[a]	18.2	44.4	36.2
γ_{us}		162	158	161
γ_{GB} (210)			966	937
γ_{GB} (310)			915	888
γ_s (111)	1790[b]	1889	1239	1231
γ_s (110)	1790[b]	2335	1475	1472
γ_s (100)	1790[b]	2149	1345	1330
γ_T	24[c]		22.2	18.2

[a]Reference 88.
[b]For average orientation, Ref. 89.
[c]Reference 90.

TABLE VI. Equilibrium cohesive energies (in eV) of selected crystalline structures of Cu predicted by the EAM potentials in comparison with TB and *ab initio* (LDA) calculations. *z* is the coordination number of the structure. * data included in the fit.

	z	*ab initio*	TB	EAM1	EAM2
fcc	12	−3.540	−3.540*	−3.540*	−3.540*
hcp[a]	12	−3.528	−3.529	−3.532*	−3.534
9R[a]	12	−3.534	−3.535	−3.535	−3.536
bcc[b]	8	−3.496	−3.500*	−3.494*	−3.494
$L1_2$	8	−3.152	−3.218	−3.124	−3.136
A15	7.5	−3.413	−3.421	−3.454	−3.447
sc[b]	6	−2.996	−3.007*	−3.107	−3.123
diamond[b]	4	−2.293	−2.429	−2.419	−2.420

[a]With ideal c/a ratio.

[b]Structure unstable against shear deformation.

surface on (111) plane, in which the energy maximum corresponds to the unstable stacking fault while the minimum at $\frac{1}{6}[\bar{2}11]$ corresponds to the stable stacking fault. TB calculations predict $\gamma_{us}=162$ mJ/m^2 in excellent agreement with EAM calculations. This agreement was also observed for other fcc metals.[36] Both potentials give very close values of surface and grain-boundary energies. The surface energies may be underestimated, which is a common feature of EAM potentials. The surface energies obtained by TB calculations are in better agreement with experiment.

V. ALTERNATIVE STRUCTURES OF CU

Besides the ground-state fcc structure, the energies of the following nonequilibrium structures of Cu were calculated by *ab initio* (LDA), TB, and EAM methods: hcp, 9R (α-Sm), bcc, $L1_2$ (fcc with one vacant site per cubic unit cell), A15 (β-W), simple cubic (sc), and diamond. The *ab initio* and TB energies were scaled as indicated in Sec. II. Table VI summarizes the equilibrium cohesive energies of the structures, ordered with increasing coordination number *z*. (For A15, the average coordination number is indicated.) The observed agreement between the energies obtained by three different methods of calculation suggests that not only the TB method but also the EAM potentials considered in this paper are transfer well to configurations far away from the ground state.

Figure 7 compares the calculated equations of state of four selected structures. Although discrepancies increase as the structure departs from the ground state, the relative stability of the structures is represented correctly by both TB and EAM methods. For the hcp and 9R structures, which are only slightly less stable than fcc, the agreement is especially good. Fig. 8 illustrates that the equations of state of the fcc and 9R structures look nearly identical. Note that, although the energy differences between the fcc, 9R, and hcp structures lie at a meV level, the trend for the cohesive energy to increase in the row fcc→9R→hcp is correctly represented by both potentials (Table VI).

The mechanical stability of the structures was evaluated by calculating the elastic constants by EAM and TB methods, and was double-checked by calculating vibrational frequencies of a large perfect lattice block using the EAM potentials. The bcc and diamond structures were found to be unstable against shear deformation with $c_{11}<c_{12}$. Likewise, the sc structure was found to be unstable against shear deformation with $c_{44}<0$. All other structures were found to be metastable.

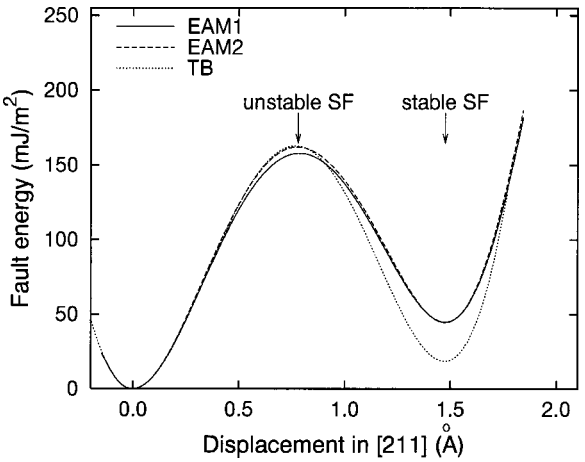

FIG. 6. Sections of the γ surface of Cu on (111) plane along $[\bar{2}11]$ direction calculated with EAM potentials and by the TB method.

Finally, Fig. 9 shows the equation of state of a Cu dimer which formally corresponds to the case of $z=1$. While both potentials agree well with *ab initio* calculations around the equilibrium [Fig. 9(a) and Table VII], the EAM2 potential shows a significant discrepancy at short distances [Fig. 9(b)]. In contrast, the EAM1 potential is accurately fit to *ab initio* energies in this range, which makes it more suitable for situations involving close approach of atoms.

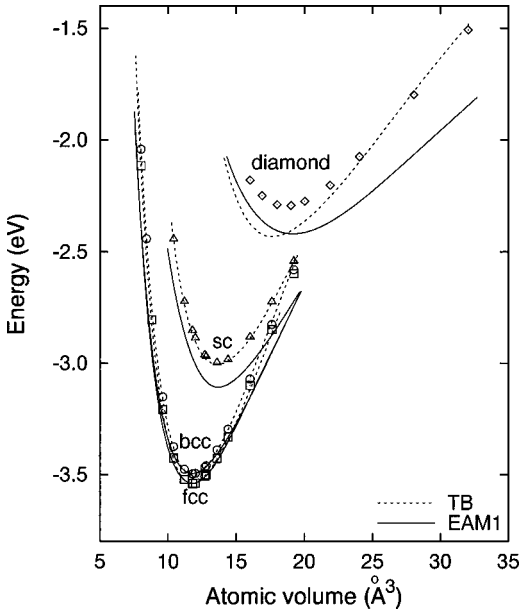

FIG. 7. Comparison of *ab initio* (LDA), TB, and EAM-calculated equations of state of the fcc (□), bcc (○), sc (△), and diamond (◇) structures of Cu around equilibrium.

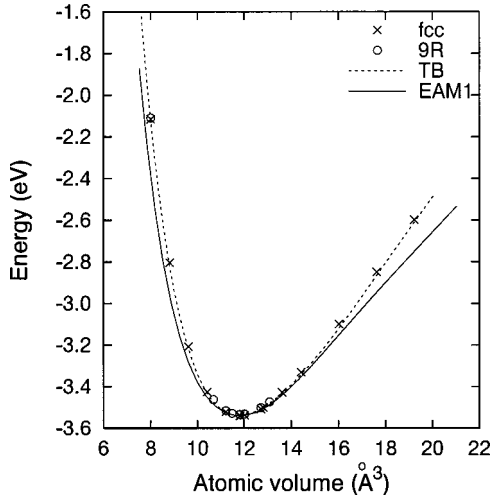

FIG. 8. Comparison of *ab initio* (LDA) (×, ○), TB, and EAM-calculated equations of state of the fcc and 9R structures. In the range shown, the equations of state of both structures are practically identical.

VI. DEFORMATION PATHS BETWEEN STRUCTURES

Energy along several deformation paths was calculated: (i) tetragonal deformation path along the Bain path[69] between the fcc and bcc structures, (ii) trigonal deformation path between the fcc, sc, and bcc structures, (iii) tetragonal deformation path going through the diamond structure, and finally (iv) (111) displacive deformation path between the fcc and 9R structures. The calculations were performed under a constant volume corresponding to the equilibrium diamond lattice in case (iii) and equilibrium fcc lattice in all other cases.

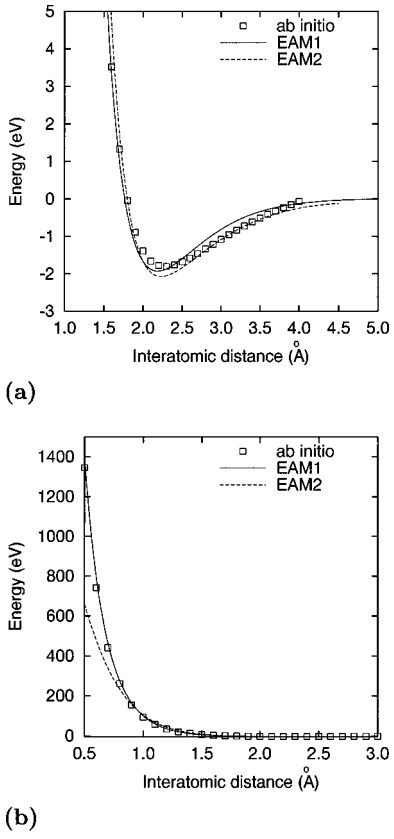

FIG. 9. Energy of a Cu dimer as a function of interatomic distance obtained by *ab initio* (B3LYP) and EAM calculations. (a) Around equilibrium. (b) At short distances.

TABLE VII. Bond length (R_d, in Å) and bond strength (E_d, in eV) of a Cu dimer predicted by the EAM potentials in comparison with experimental data and *ab initio* (GGA) calculations.

	Experiment	*ab initio*	EAM1	EAM2
R_d	2.2[a]	2.32	2.18	2.24
E_d	−2.05[a]	−1.80	−1.93	−2.07

[a]Reference 91.

A. Bain path

Under the Bain deformation,[1–9,18,70,71] the initial fcc lattice ($c/a=1$) is compressed along [001] direction and simultaneously expanded to an equal extent in [100] and [010] directions so as to preserve the atomic volume. At $c/a=1/\sqrt{2}$ the lattice becomes bcc. All three calculation methods employed in this work predict a maximum of the energy at $c/a=1/\sqrt{2}$ (Fig. 10), thus indicating that the bcc structure is unstable against tetragonal deformation. This instability is consistent with the negative shear modulus $C'=(c_{11}-c_{12})/2$ found for the bcc structure. The shallow minimum observed at $c/a<1/\sqrt{2}$ corresponds to a body-centered-tetragonal (bct) structure which is stable against tetragonal distortions but turns out to be unstable against other modes of shear deformation. This structure is known[72] as A_a and can be truly metastable in other metals, for example in highly compressed Sn.

B. Trigonal deformation path

The trigonal deformation path[8,9,18,71,73] is simulated by applying to the fcc structure a tensile strain in the [111] direc-

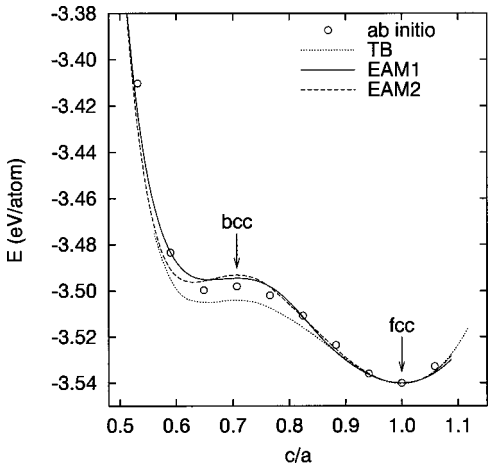

FIG. 10. Comparison of *ab initio* (LDA), TB, and EAM calculations of energy along the Bain path between fcc and bcc structures. Calculations were performed at a constant volume corresponding to the equilibrium fcc phase.

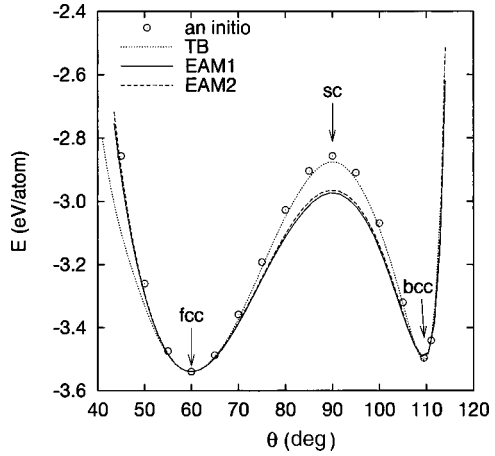

FIG. 11. Comparison of *ab initio* (LDA), TB, and EAM calculations of energy along the trigonal deformation path. Calculations were performed at a constant volume corresponding to the equilibrium fcc phase.

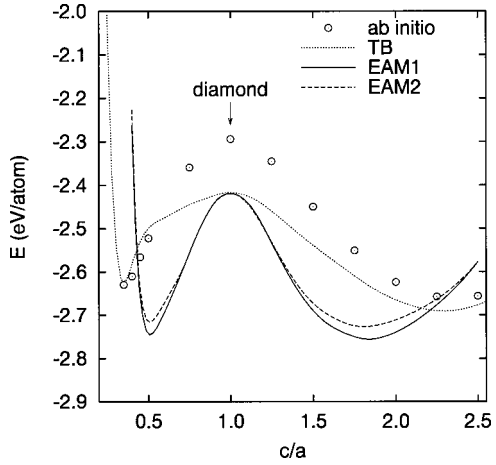

FIG. 12. Comparison of *ab initio* (LDA), TB, and EAM calculations of the energy of diamond Cu along the tetragonal deformation path. Calculations were performed at a constant volume corresponding to the equilibrium diamond structure.

tion with a simultaneous compression in the $[\bar{2}11]$ and $[01\bar{1}]$ directions in such a way that to maintain the threefold rotational symmetry around the [111] direction and preserve the atomic volume. The degree of deformation can be measured by the angle, θ, between the primitive translation vectors of the lattice, with $\theta=60°$ corresponding to the fcc structure. Figure 11 shows the energy along this deformation path. Again, all three calculation methods predict a maximum at $\theta=90°$ (sc structure) and a minimum at $\theta=109.5°$ (bcc structure). This plot demonstrates that the bcc structure is stable ($c_{44}>0$) while the sc structure is unstable ($c_{44}<0$) against trigonal distortions.

C. Tetragonal deformation of the diamond structure

The EAM and TB calculations predict that the diamond structure of Cu is elastically unstable with $c_{11}<c_{12}$. In order to verify this instability by *ab initio* calculations, the energy of the diamond structure was calculated as a function of c/a along a volume-conserving tetragonal deformation path. The occurrence of a maximum at $c/a=1$, predicted by all calculation methods (Fig. 12), confirms that diamond Cu is unstable against tetragonal distortions. The structures corresponding to the local minima on either side of the maximum are unstable against other modes of deformation. Although they do not represent any known crystalline structures, they are likely to lie in energy basins corresponding to some metastable structures in the full configuration space. The identification of those metastable structures was not pursued in this work.

D. fcc→9R transformation

For modeling this transformation we first followed the scheme outlined in Ref. 9. As the initial configuration, we used a 9-atomic supercell representing the stacking sequence ABCABCABC of (111) planes characteristic of the fcc structure. While keeping the first three (111) planes intact, the next three planes were shifted by the amount of $\xi a_0/\sqrt{6}$ in the $[\bar{2}11]$ direction, whereas the following three planes were shifted by the same amount in the opposite direction, $[2\bar{1}\bar{1}]$. At $\xi=1$ we arrive at the stacking sequence ABCBCACAB corresponding to the 9R structure. We refer to this transformation path as Path 1. Because dimensions of the supercell do not change, the atomic volume is conserved. Internal atomic relaxations were not allowed either. In this regime, the energy calculations were performed by the EAM and TB methods and yielded similar results (Fig. 13). The 9R structure was found to be metastable, which was mentioned in Ref. 9 as a possibility. Note the difference between this transformation path, on one hand, and the previously considered tetragonal and trigonal deformation paths, on the other hand. While the tetragonal and trigonal deformations are homogeneous and correspond to long-wavelength phonons, the fcc→9R transformation is initiated by a transverse $[\frac{1}{3},\frac{1}{3},\frac{1}{3}]$ phonon in the fcc structure. A similar scheme, involving $\xi[211]$-type displacements of (111) planes, could be developed for modeling an fcc→hcp transformation. Note also that the barrier of the fcc→9R transformation along this path is relatively high (~100 meV), in general agreement with previous *ab initio* calculations.[9] We did not perform our own *ab initio* calculations for this path: because they are computationally expensive, and because we found an easier path that can be modeled with a 3-atom supercell.

For this path, which we call Path 2, we choose the lattice translation vectors as

$$\left(\frac{a_0}{2},-\frac{a_0}{2},0\right)$$

$$\left(0,\frac{a_0}{2},-\frac{a_0}{2}\right)$$

$$(a_0,a_0,a_0)+\xi\left(\frac{a_0}{6},\frac{a_0}{6},-\frac{a_0}{3}\right)$$

and the basis vectors as

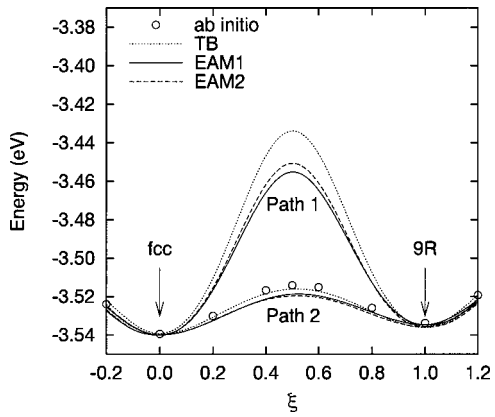

FIG. 13. Energy along two displacive deformation paths between the fcc and 9R structures described in the text. ξ is the normalized displacement along the path.

$$(0,0,0)$$

$$\left(\frac{a_0}{2},0,\frac{a_0}{2}\right)$$

$$\left(-\frac{a_0}{2},0,-\frac{a_0}{2}\right).$$

Then, we have the fcc structure at $\xi=0$ and the 9R structure at $\xi=1$. Again, no relaxation was included in the calculation. Like Path 1 considered before, this transformation is nonhomogeneous and involves certain short-wave phonons. For this path, calculations were performed by all three methods and gave very consistent results (Fig. 13). We note, however, that the barrier of Path 2 is only $\sim$20 meV, i.e., much lower than for Path 1. Lattice relaxations are likely to make this barrier even lower. This low barrier for the fcc$\rightarrow$9R transformation correlates with the fact that layers of the 9R structure were observed at grain boundaries on several occasions.[11,12]

VII. APPLICATION TO STRUCTURE OF EPITAXIAL FILMS

A. Transformations between fcc, bcc, and hcp structures under epitaxial constraints

During a pseudomorphic film growth, the grown material tends to adopt the structure of the substrate, or at least a structure that provides the best match to the uppermost atomic layer of the substrate. This structure can be a strained ground-state structure or some other (but usually also strained) nonequilibrium structure. The occurrence of a particular structure depends[70] on its equilibrium energy relative to the ground state, the strain energy which accommodates the deviation of the lattice period from its equilibrium value, the mechanical stability of the structure, and the relevant interfacial energies. The structures of fcc metals grown epitaxially on (001)-oriented fcc or bcc substrates were experimentally identified as strained fcc,[6,7,74] bct,[15,16,75,76] or hcp (Ref. 16) structures. In this section we present a simple model allowing us to predict the most favorable structure of a Cu film growing epitaxially on a (001) substrate, depending on the lattice period of the substrate. The calculations employ the EAM1 potential.

In order to describe transitions among the fcc, bcc, and hcp structures of the film, we first consider an orthorhombic lattice with translation vectors

$$(a,0,0)$$

$$(0,b,0)$$

$$(0,0,c)$$

and basis vectors

$$(0,0,0)$$

$$\left(\frac{a}{2},0,\frac{c}{2}\right)$$

$$\left(\xi\frac{a}{6},\frac{b}{2},\frac{c}{2}\right)$$

$$\left(\frac{a}{2}+\xi\frac{a}{6},\frac{b}{2},0\right),$$

where ξ is an internal parameter of the structure. We assume that the (001) (i.e., a–b) plane of the structure is parallel to the substrate. This general structure reduces to an fcc structure with lattice period a_{fcc} when

$$a=b=c=a_{\mathrm{fcc}},\quad \xi=0, \tag{17}$$

to a bcc structure with lattice period a_{bcc} when

$$a=b=\sqrt{2}a_{\mathrm{bcc}},\quad c=a_{\mathrm{bcc}},\quad \xi=0, \tag{18}$$

and to an hcp structure with lattice spacing a_{hcp} in basal planes and an ideal $c_{\mathrm{hcp}}/a_{\mathrm{hcp}}$ ratio when

$$a=\sqrt{3}a_{\mathrm{hcp}},\quad b=\sqrt{8/3}a_{\mathrm{hcp}},\quad c=a_{\mathrm{hcp}},\quad \xi=\pm 1. \tag{19}$$

Note that the c-axis [0001] and the prismatic plane $(11\bar{2}0)$ of the hcp structure are parallel to the substrate, which is consistent with the orientation observed experimentally.[16]

The energy of the described orthorhombic structure is a function of four variables a, b, c, and ξ. However, the epitaxy condition imposes constraints on possible configurations. Namely, a and b must be equal to each other and coincide with the lattice period of the fcc substrate or $\sqrt{2}$ times the lattice period of the bcc substrate. Thus, the energy becomes a function of only two variables, c/a and ξ. In this constrained configuration space, we obtain an fcc structure of the film when

$$c/a=1,\quad \xi=0, \tag{20}$$

a bcc structure when

$$c/a=1/\sqrt{2},\quad \xi=0, \tag{21}$$

and a deformed hcp structure when

TABLE VIII. Lattice periods of the fcc(001) and bcc(001) substrates that are expected to favor the fcc, bcc, and hcp structures of a pseudomorphic film. a_0 is the equilibrium fcc lattice period of the growing material.

	Substrate structure	
Film structure	fcc	bcc
fcc	$a_{fcc}=a_0$	$a_{bcc}=a_0/\sqrt{2}\approx 0.707a_0$
bcc	$a_{fcc}=(2/\sqrt{3})a_0\approx 1.155a_0$	$a_{bcc}=\sqrt{2/3}a_0\approx 0.817a_0$
hcp	$a_{fcc}=\sqrt{3/2}a_0\approx 1.225a_0$	$a_{bcc}=(\sqrt{3}/2)a_0\approx 0.866a_0$

$$c/a=1/\sqrt{3},\quad \xi=\pm 1. \tag{22}$$

Note that the hcp structure now has a nonideal c_{hcp}/a_{hcp} ratio of $\sqrt{3}$, which is about 6% larger than the ideal ratio of $\sqrt{8/3}$.

Before any calculations, we can estimate the lattice periods of the fcc(001) and bcc(001) substrates that can be expected to favor the fcc, bcc, and hcp structures of an epitaxial film (Table VIII). These estimates are based on the assumption that the first-neighbor distances in the bcc structure and in basal planes of the hcp structure of the film tend to be close to the equilibrium first-neighbor distance, $a_0/\sqrt{2}$, in the fcc phase, which is, of course, an approximation. Table VIII also eludes to the mechanical instability of the bcc structure. For example, for a W(001) substrate we have $a_{bcc}/a_0\approx 0.876$ (using $a_{bcc}=3.165$ Å),[77] which indicates that this substrate must strongly favor the hcp structure of Cu. The hcp structure was indeed found experimentally in the Cu/W(001) system with the orientation predicted by this model.[16] For a Pd(001) substrate we have $a_{fcc}/a_0\approx 1.076$ (using $a_{fcc}=3.89$ Å),[77] a value lying between the substrate lattice periods that favor the fcc and bcc structures of a Cu film. This transient character of the situation may explain the controversy regarding the film structure, which was interpreted by different authors as either strained fcc or strained bcc.[6,7,15]

To obtain more insight into transitions between different structures of a film, the energy was calculated as a function of c/a and ξ for various values of a/a_0. For a/a_0 values slightly above unity, the energy has only one minimum at $\xi=0$ and some $c/a<1$. Note that the hcp structure remains unstable.[78] As a/a_0 increases, c/a decreases, and the system is essentially driven along the so-called epitaxial Bain path.[7] An example of this behavior is shown in Fig. 14(a), where the energy contours in the c/a-ξ space were calculated for the value of $a/a_0=1.08$ corresponding to Cu/Pd(001).[15] At a critical value of $a/a_0\approx 1.112$, the system reaches a bifurcation point at which the minimum at $\xi=0$ and $c/a\approx 0.73$ turns into a saddle point, while two minima corresponding to symmetrically equivalent strained hcp structures ($\xi\neq 0$) appear at the energy surface [Fig. 14(b)]. As a/a_0 increases further, the internal parameter ξ of the hcp structure increases and tends to ± 1, while the c/a ratio decreases and tends to the value $1/\sqrt{3}$ predicted by Eq. (22). The energy contours for $a/a_0=1.24$ [the case of Cu/W(001)][16] indicate that the deformation of the obtained hcp structure is relatively small [Fig. 14(c)].

Thus, the calculations predict that, at a given film/substrate mismatch a/a_0, only one structure (out of three considered) can be metastable: either deformed fcc or deformed hcp, depending upon a/a_0. The bcc structure always remains unstable, and must spontaneously transform to either fcc or hcp. This transformation involves a compression of the film in the direction normal to the substrate, which is controlled by parameter c/a. The transformation to the hcp phase also involves a relative displacement of sublattices in $[110]_{bcc}$ direction parallel to the substrate, which is controlled by parameter ξ. The latter mode of deformation is associated with a transverse phonon $(\frac{1}{2},\frac{1}{2},0)$. These deformation modes cannot be prevented by the substrate.

B. Atomistic simulation of epitaxial structures

In order to verify the analysis of Sec. VII A, the structures of epitaxial Cu films were determined by atomistic simulations using the EAM1 potential. A slab of fcc Cu with (001) orientation was created as the initial configuration. The atoms of the first 13 (002) layers were treated as ''free'' atoms, i.e., were allowed to move, while all other atoms were fixed in their perfect-lattice positions. The thickness of the fixed layer was at least twice the cutoff radius of atomic interaction. The fixed layer simulated an infinitely thick fcc(001) substrate. Periodic boundary conditions were imposed in the [100] and [010] directions parallel to the slab. The initial lattice period was a_0. Before the simulation, the system was uniformly expanded by a making the lattice period equal $a>a_0$. Molecular dynamics was then run on ''free'' atoms at temperature 500 K for about a nanosecond, followed by static relaxation. This procedure served to destroy the symmetry of the initial configuration and find a minimum of the potential energy.

As expected from the previous analysis, the film structure was always found to be either fcc or hcp, depending on the lattice mismatch a/a_0. For example at $a/a_0=1.07$, the structure was found to be a deformed fcc with $c/a\approx 0.8$ [Fig. 15(a)] in agreement with calculations in Sec. VII A. Geometrically, this structure lies between fcc and bcc, which was recognized experimentally for Cu/Pd(001).[6,7,15] On the other hand, at $a/a_0=1.24$ the structure is hcp [Fig. 15(b)], again in agreement with previous calculations (Sec. VII A) and experimental observations.[16] The orientation of the hcp phase relative to the substrate is also consistent with experiments on Cu/W(001).[16]

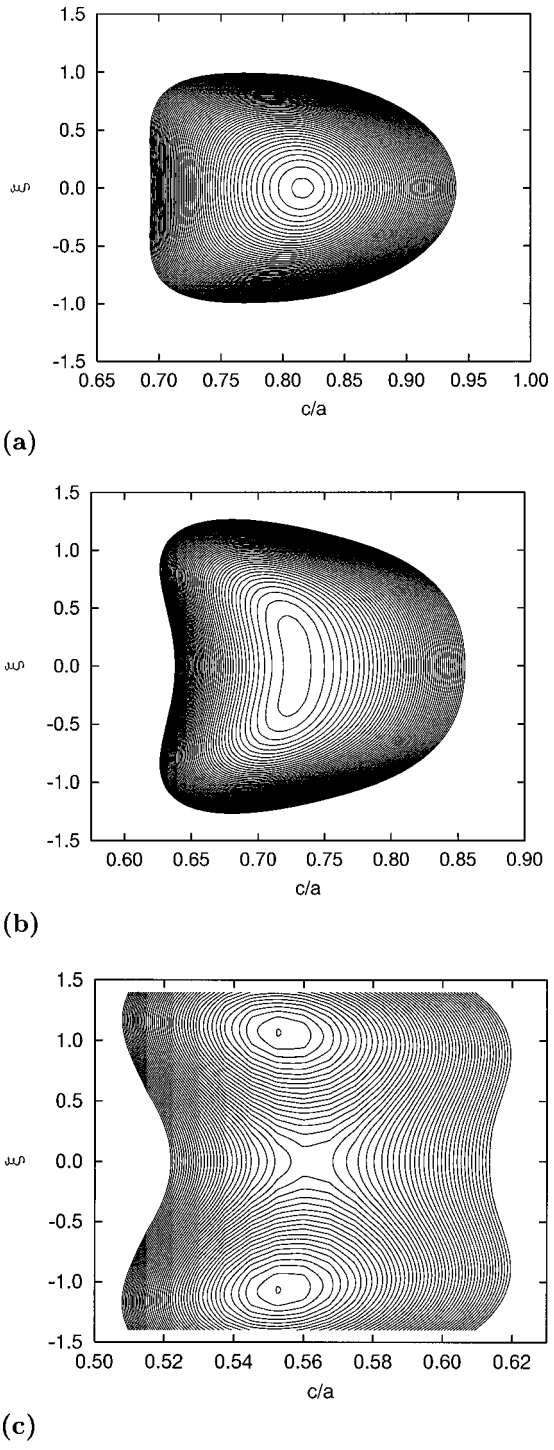

FIG. 14. Constant energy contours for an epitaxially constrained orthorhombic Cu structure calculated with the EAM1 potential. ξ and c/a are deformation parameters of the structure. The contours are shown in every 0.002 eV between -3.54 and -3.40 eV. (a) $a/a_0=1.08$; the single minimum corresponds to a deformed fcc structure. (b) $a/a_0=1.112$; situation close to the bifurcation point at which the minimum splits. (c) $a/a_0=1.24$; the two minima represent an hcp structure while the saddle point corresponds to the unstable bcc phase.

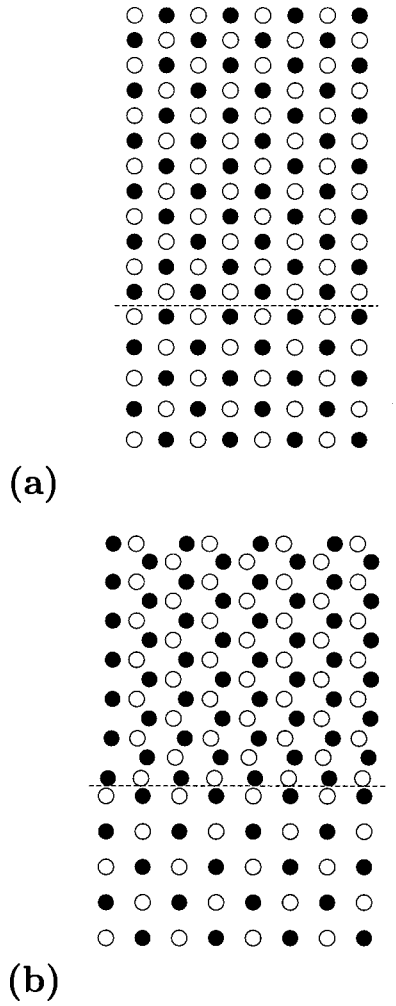

FIG. 15. Simulated structures of epitaxial Cu films on an fcc(001) substrate. The filled and open circles mark atomic positions in alternating (200) planes. The dashed line shows the interface between the substrate (below the line) and the film (above the line). The $[010]_{fcc}$ direction is normal to the paper. (a) $a/a_0=1.07$; the film has a deformed fcc structure. (b) $a/a_0=1.24$; the film has an hcp structure.

VIII. SUMMARY

Ab initio methods are recognized to be accurate for the evaluation of energies and mechanical stability of not only equilibrium but also nonequilibrium crystalline structures of metals.[1,2] The recently developed total-energy TB method[17,18] is also suitable for nonequilibrium structure calculations. Although this has been demonstrated in previous work,[17,18] this paper provides further proof of transferability of TB calculations by taking Cu as a model material. Excellent agreement is observed between *ab initio* and TB data for the energy and stability of several nonequilibrium structures of Cu, including highly nonequilibrium structures such as diamond. This agreement also extends to various transformation paths between different structures calculated in this work.

It was interesting to investigate how reliable the embedded-atom method is for this purpose. We did this investigation with two potentials. One of them (EAM1) has

been constructed in this work by using more fitting parameters and a larger fitting database (including experimental and *ab initio* data) than usual. The other potential (EAM2) was constructed previously[21,22] using a traditional scheme based on fewer fitting parameters and experimental data only. The potentials have been extensively tested by calculating fcc lattice properties, point and extended defects, various structural energies, and transformation paths. The EAM1 potential appears to be somewhat more accurate than EAM2 for lattice defect simulations, and certainly more accurate for simulations involving a close approach of atoms (such as sputtering simulations). The latter feature of the EAM1 potential is due to the incorporation of *ab initio* energies corresponding to short atomic separations in its fitting database. However, with respect to the energetics and stability of nonequilibrium structures both potentials perform equally well and show excellent agreement with both *ab initio* and TB calculations.

This agreement allows us to conclude that EAM potentials *can be* quite reliable for simulations in which correct energies and stability of different atomic configurations are of prime importance for obtaining credible results. Such potentials can be safely applied for atomistic simulations of extended defect cores, epitaxial film structure, etc. We are not stating that *every* EAM potential will correctly represent nonequilibrium structures. We only conclude that the two Cu potentials examined here possess this quality. Further investigations will show how well EAM potentials perform in this respect for other metals. The recent results for Ni and Al EAM potentials look very encouraging.[8,20]

The elastic instability of the bcc and sc structures of fcc metals has been identified previously[1–9] by calculating tetragonal and trigonal deformation paths in which these structures produced energy maxima. This instability was confirmed in this work, but it should be recognized that the relevant maxima of energy are symmetry dictated, so it can be argued that every reasonable atomic interaction model must reproduce them as long as the structural energies increase in the row fcc→bcc→sc. It was less obvious that the diamond structure would be elastically unstable, but this fact was established here by *ab initio*, TB, and EAM methods. At the same time, the hcp, 9R, A15, and $L1_2$ structures were found to be metastable. These observations suggest that only structures obtainable from fcc by introducing point defects (e.g., vacancies like in $L1_2$) or planar faults (e.g., stacking faults like in hcp and 9R) can be metastable, while all structures that can be obtained from fcc or the metastable structures by homogeneous deformation are always unstable. This rule seems to work for Cu, but further investigations are required for its corroboration.

As an application of our analysis, we carried out EAM calculations of nonequilibrium structures that can be found in Cu films grown epitaxially on (001)-oriented fcc or bcc substrates. We applied a simple model describing the energetics and stability of fcc, bcc, and hcp structures of the film based on bulk-crystal calculations. The model predicts that only deformed fcc and hcp structures can be adopted by the film, depending on the lattice mismatch with the substrate. The bcc structure remains unstable and cannot be stabilized by the epitaxial constraints. These predictions are confirmed by atomistic simulation results, which are consistent with experimental observations.[6,7,15,16]

ACKNOWLEDGMENTS

The authors are grateful to the U.S. Department of Energy (US DOE), Office of Basic Energy Sciences, for financial support, including Grant No. DE-FG02-99ER45769 (Y.M.). The work at Los Alamos National Laboratory was carried out under the auspices of the US DOE (Contract No. W-7405-ENG-36). M.J.M. and D.A.P. were supported by the U.S. Office of Naval Research. The development of the tight-binding and atomistic-simulation codes and parameters was supported in part by the U.S. Department of Defense Common HPC Software Support Initiative (CHSSI). The tight-binding calculations included here were supported in part by a grant of HPC time from the DoD HPC Modernization Office, for computations on the IBM SP2 and SGI Origin at the Aeronautical Systems Center, Wright-Patterson Air Force Base, Dayton, OH. A.F.V. and J.D.K. thank Dr. C. Greeff for useful discussions regarding the equation of state of copper and for providing the diamond anvil cell data shown in Fig. 5.

[1] P. J. Craievich, M. Weinert, J. M. Sanchez, and R. E. Watson, Phys. Rev. Lett. **72**, 3076 (1994).
[2] P. J. Craievich, J. M. Sanchez, R. E. Watson, and M. Weinert, Phys. Rev. B **55**, 787 (1997).
[3] G. W. Fernando, J. Mei, R. E. Watson, M. Weinert, and J. W. Davenport, Phys. Rev. B **47**, 13 636 (1993).
[4] T. Kraft, P. M. Marcus, M. Methfessel, and M. Scheffler, Phys. Rev. B **48**, 5886 (1993).
[5] A. Y. Liu and D. J. Singh, Phys. Rev. B **47**, 8515 (1993).
[6] S. Jeong, Phys. Rev. B **53**, 13 973 (1996).
[7] P. Alippi, P. M. Marcus, and M. Scheffler, Phys. Rev. Lett. **78**, 3892 (1997).
[8] Y. Mishin, D. Farkas, M. J. Mehl, and D. A. Papaconstantopoulos, Phys. Rev. B **59**, 3393 (1999).
[9] L. G. Wang and M. Sŏb, Phys. Rev. B **60**, 844 (1999).
[10] E. G. Moroni, G. Grimvall, and T. Jarlborg, Phys. Rev. Lett. **76**, 2758 (1996).
[11] U. Wolf, F. Ernst, T. Muschik, M. W. Finnis, and H. F. Fischmeister, Philos. Mag. A **66**, 991 (1992).
[12] F. Ernst, M. W. Finnis, D. Hofmann, T. Muschik, U. Schonberger, U. Wolf, and M. Methfessel, Phys. Rev. Lett. **69**, 620 (1992).
[13] C. Schmidt, F. Ernst, M. W. Finnis, and V. Vitek, Phys. Rev. Lett. **75**, 2160 (1995).
[14] C. Schmidt, F. Ernst, M. W. Finnis, and V. Vitek, Philos. Mag. A **77**, 1161 (1998).
[15] E. Hahn, E. Kampshoff, N. Wälhcli, and K. Kern, Phys. Rev. Lett. **74**, 1803 (1995).

[16] H. Wormeester, E. Hüger, and E. Bauer, Phys. Rev. Lett. **77**, 1540 (1996).
[17] R. E. Cohen, M. J. Mehl, and D. A. Papaconstantopoulos, Phys. Rev. B **50**, 14 694 (1994).
[18] M. J. Mehl and D. A. Papaconstantopoulos, Phys. Rev. B **54**, 4519 (1996).
[19] M. S. Daw and M. I. Baskes, Phys. Rev. B **29**, 6443 (1984).
[20] Y. Mishin, D. Farkas, M. J. Mehl, and D. A. Papaconstantopoulos, in *Multiscale Modelling of Materials*, edited by V. V. Bulatov, T. Diaz de la Rubia, R. Phillips, E. Kaxiras, and N. Ghoniem, MRS Symposia Proceedings No. 535 (Materials Research Society, Warrendale, Pennsylvania, 1999).
[21] A. F. Voter, Los Alamos Unclassified Technical Report No. LA-UR 93-3901, 1993 (unpublished).
[22] A. F. Voter, Phys. Rev. B **57**, R13 985 (1998).
[23] S. M. Foiles, M. I. Baskes, and M. S. Daw, Phys. Rev. B **33**, 7983 (1986).
[24] D. J. Oh and R. A. Johnson, J. Mater. Res. **3**, 471 (1988).
[25] R. A. Johnson, Phys. Rev. B **37**, 3924 (1988).
[26] R. A. Johnson, Phys. Rev. B **37**, 6121 (1988).
[27] J. B. Adams, S. M. Foiles, and W. G. Wolfer, J. Mater. Res. **4**, 102 (1989).
[28] C. L. Rohrer, Modell. Simul. Mater. Sci. Eng. **2**, 119 (1994).
[29] M. Doyama and Y. Kogure, Comput. Mater. Sci. **14**, 80 (1999).
[30] O. K. Andersen, Phys. Rev. B **12**, 3060 (1975).
[31] S. H. Wei and H. Krakauer, Phys. Rev. Lett. **55**, 1200 (1985).
[32] J. P. Perdew and Y. Wang, Phys. Rev. B **45**, 13 244 (1992).
[33] W. Kohn and L. J. Sham, Phys. Rev. **140**, A1133 (1965).
[34] D. D. Koelling and B. N. Harmon, J. Phys. C **10**, 3107 (1977).
[35] M. J. Gillan, J. Phys.: Condens. Matter **1**, 689 (1989).
[36] M. J. Mehl, D. A. Papaconstantopoulos, N. Kioussis, and M. Herbranson, Phys. Rev. B **61**, 4894 (2000).
[37] M. J. Mehl, Phys. Rev. B **61**, 1654 (2000).
[38] G. Kresse and J. Hafner, Phys. Rev. B **47**, 558 (1993).
[39] G. Kresse and J. Furthmüller, Comput. Mater. Sci. **6**, 15 (1996).
[40] G. Kresse and J. Furthmüller, Phys. Rev. B **54**, 11 169 (1996).
[41] J. P. Perdew, J. A. Chevary, S. H. Vosko, K. A. Jackson, M. R. Pedersen, D. J. Singh, and C. Fiolhais, Phys. Rev. B **46**, 6671 (1992).
[42] D. Vanderbilt, Phys. Rev. B **41**, 7892 (1990).
[43] G. Kresse and J. Hafner, J. Phys.: Condens. Matter **6**, 8245 (1994).
[44] A. D. Becke, J. Chem. Phys. **98**, 5648 (1993).
[45] C. Lee, W. Yang, and R. G. Parr, Phys. Rev. B **37**, 785 (1988).
[46] B. Miehkuch, A. Savin, H. Stoll, and H. Preuss, Chem. Phys. Lett. **157**, 200 (1989).
[47] M. J. Frisch *et al.*, *Gaussian 98 Revision A.6* (Gaussian Inc., Pittsburgh, PA, 1998).
[48] The TB programs and parameters are available for retrieval by FTP from http://cst-www.nrl.navy.mil/bind/dodtb
[49] N. Bernstein, M. J. Mehl, D. A. Papaconstantopoulos, N. I. Papanicolaou, M. Z. Basant, and E. Kaxiras, Phys. Rev. B **62**, 4477 (2000).
[50] F. Kirchhoff, M. J. Mehl, N. I. Papanicolaou, D. A. Papaconstantopoulos, and F. S. Khan, Phys. Rev. B **63**, 195101 (2001).
[51] Physically, it is only the structural energy *differences* calculated by different methods that can be compared with each other. By taking all energies to the same reference we only simplify the terminology by eliminating the word ''differences,'' but the physical meaning of the energies remains the same.
[52] A. F. Voter, *Intermetallic Compounds* (John Wiley & Sons, New York, 1994), Vol. 1, Chap. 4, p. 77.
[53] R. A. Johnson, in *Many Atom Interactions*, Proceedings in Physics Vol. 48 (Springer-Verlag, Berlin, 1990).
[54] J. H. Rose, J. R. Smith, F. Guinea, and J. Ferrante, Phys. Rev. B **29**, 2963 (1984).
[55] S. M. Foiles, Phys. Rev. B **32**, 7685 (1985).
[56] The potential functions are available for retrieval by FTP at http://cst-www.nrl.navy.mil/bind/cu.html
[57] G. Nilsson and S. Rolandson, Phys. Rev. B **7**, 2393 (1973).
[58] J. N. Murrell, Philos. Mag. A **73**, 163 (1996).
[59] S. M. Foiles, Phys. Rev. B **49**, 14 930 (1994).
[60] S. M. Foiles and J. B. Adams, Phys. Rev. B **40**, 5909 (1989).
[61] P. M. Bell, J. Xu, and H. K. Mao, in *Shock Waves in Condensed Matter*, edited by Y. M. Gupta (Plenum Press, New York/London, 1985) p. 125.
[62] J. Xu, H. K. Mao, and P. M. Bell, High Temp.-High Press. **16**, 495 (1984).
[63] H. Jónsson, G. Mills, and K. W. Jacobsen, in *Classical and Quantum Dynamics in Condensed Phase Simulations*, edited by B. J. Berne, G. Ciccotti, and D. F. Coker (World Scientific, Singapore, 1998) p. 1.
[64] G. H. Vineyard, J. Phys. Chem. Solids **3**, 121 (1957).
[65] R. W. Balluffi, J. Nucl. Mater. **69&70**, 240 (1978).
[66] J. R. Rice, J. Mech. Phys. Solids **40**, 239 (1992).
[67] V. Vitek, Philos. Mag. **73**, 773 (1968).
[68] V. Vitek, Cryst. Lattice Defects **5**, 1 (1974).
[69] E. C. Bain, Trans. AIME **70**, 25 (1924).
[70] V. Ozoliņš, C. Wolverton, and A. Zunger, Phys. Rev. B **57**, 4816 (1998).
[71] M. Sŏb, L. G. Wang, and V. Vitek, Comput. Mater. Sci. **8**, 100 (1997).
[72] More information on this structure is available at http://cst-www.nrl.navy.mil/lattice/struk/a_a.html
[73] S. Fox and H. J. F. Jansen, Phys. Rev. B **53**, 5119 (1996).
[74] C. Path, J. E. Prieto, S. Müller, R. Miranda, and K. Heinz, Phys. Rev. B **55**, 10 791 (1997).
[75] N. Metoki, W. Donner, and H. Zabel, Phys. Rev. B **49**, 17 351 (1994).
[76] Z. Q. Wang, S. H. Lu, D. Tian, Y. S. Li, F. Jona, and P. M. Markus, Phys. Rev. B **35**, 9322 (1987).
[77] C. Kittel, *Introduction to Solid State Physics* (Wiley-Interscience, New York, 1986).
[78] This statement refers to the strongly deformed hcp structure and does not contradict to the fact that the equilibrium hcp phase is metastable.
[79] *Metal Reference Book*, 5th ed., edited by C. J. Smith (Butterworth, London, 1976).
[80] G. Simons and H. Wang, *Single Crystal Elastic Constants and Calculated Aggregate Properties* (MIT Press, Cambridge, MA, 1977).
[81] *Metals: Phonon States, Electron States, and Fermi Surfaces*, edited by K.-M. Hellwege and J. L. Olson, Landolt-Bornstein, New Series, Group III, Vol. 13a (Springer, Berlin, 1981).
[82] R. W. Siegel, J. Nucl. Mater. **69&70**, 117 (1978).
[83] P. Ehrhart, J. Nucl. Mater. **69&70**, 200 (1978).
[84] M. Beyeler and Y. Adda, J. Phys. (France) **29**, 345 (1968).
[85] P. B. McArdle, Bull. Am. Phys. Soc. **13**, 489 (1968).

[86] *Properties and Interaction of Atomic Defects in Metals and Alloys*, edited by H. Ullmaier, Landolt-Bornstein, New Series, Group III, Vol. 25 (Springer, Berlin, 1991).
[87] F. W. Young, J. Nucl. Mater. **69&70**, 310 (1978).
[88] C. B. Carter and I. L. F. Ray, Philos. Mag. **35**, 189 (1977).
[89] W. R. Tyson and W. R. Miller, Surf. Sci. **62**, 267 (1977).
[90] L. E. Murr, *Interfacial Phenomena in Metals and Alloys* (Addison-Wesley, Reading, MA, 1975).
[91] K. P. Huber and G. Hertzberg, *Constants of Diatomic Molecules* (Van Nostrand Reinhold, New York, 1979).
[92] *Thermal Expansion, Metallic Elements and Alloys, Vol. 12 of Thermophysical Properties of Matter*, edited by Y. S. Touloukian, R. K. Kirby, R. E. Taylor, and P. D. Desai (Plenum, New York-Washington, 1975).